Mathematical Biosciences and Engineering

MBE, 16(6): 7405–7420.
DOI: 10.3934/mbe.2019370
Received: 30 April 2019
Accepted: 07 August 2019
Published: 14 August 2019

http://www.aimspress.com/journal/MBE

Research article

Optimization of surgical protocol for laser iridotomy based on the numerical simulation of aqueous flow

Yibo Zhao, Bin Chen* and Dong Li

State Key Laboratory of Multiphase Flow in Power Engineering, Xi'an Jiaotong University, Xi'an, Shanxi, China

*** Correspondence:** Email: chenbin@mail.xjtu.edu.cn; Tel: +8602982667326; Fax: +8602982669033.

Abstract: Primary angle-closure glaucoma (PACG) is a major cause of blindness worldwide, with a particularly high prevalence in Asian populations. Laser iridotomy (LI) has been the standard therapeutic modality for treating PACG to avoid blindness. However, the complex structure of the eyeball, the aqueous fluidity, and the limitation of detecting equipment will cause difficulty in surgery and the probability of complications. Numerical simulation was conducted to investigate aqueous humor (AH) flow under different physiological structures before and after laser surgery. When the anterior chamber depth decreases from 2.8 mm to 2.0 mm (caused by angle-closure glaucoma), the maximum velocity of natural convection is doubled, and the pressure difference between the posterior and anterior chambers increases by 20%. Therefore, a shallow anterior chamber depth is crucial for the accurate investigation of glaucoma. Pupil block sharply increases the intraocular pressure (IOP). When the gap between the lens and iris decreases from 10 μm to 0.5 μm, P between the posterior and anterior chambers is approximately 37 times higher than before, thereby damaging intraocular tissues. LI can effectively reduce the IOP caused by pupil block, but the velocity of AH after operation is 40 times the normal condition, and the increased corneal shear stress could lead to corneal damage, which can be solved by adjusting the incident angle of laser beam On the basis of the allowable angle range of surgical equipment and the effect of different incident angles on the cornea and iris, the optimum angle of laser drilling is 45 °.

Keywords: primary angle-closure glaucoma; laser iridotomy; aqueous humor flow; numerical simulation; pupil block

1. Introduction

Primary angle-closure glaucoma (PACG) is a major cause of blindness worldwide, with a particularly high prevalence in Asian populations. The number of people with PACG is estimated to increase to 23.4 million in 2020, of whom 76.7% will be Asian [1]. PACG refers to the blocking of trabecular meshwork by the peripheral iris; thus, the anterior chamber angle is closed, and the aqueous outflow is obstructed, thereby increasing the intraocular pressure (IOP) beyond the tolerance degree of the eyeball. PACG will lead to optic nerve atrophy, visual field shrinkage, visual impairment, and even blindness.

The pathogenesis of glaucoma is closely related to the abnormal flow of aqueous humor (AH), which inflates the globe of the eye while maintaining the IOP. AH provides the required nutrition for the avascular ocular tissues, posterior cornea, trabecular meshwork, lens, and anterior vitreous. The anterior chamber, as a space inside the eye between the iris and innermost surface of the cornea, is filled with AH, as shown in Figure 1. The ciliary body secretes the AH into the posterior chamber at a rate of approximately 1.5–3.0 μL/min. Then, this fluid flows through the narrow cleft between the lens and iris and escapes through the pupil into the anterior chamber. Finally, the AH drains out of the eye via the trabecular meshwork, and its residence time in the eyeball is approximately 100 min [2]. Only when the anterior chamber is in a certain depth can AH be discharged smoothly, and the IOP can be maintained within the normal range. However, the anterior chamber of angle-closure glaucoma is often shallow, which is not conducive to AH discharge and easily increases the IOP. In addition, pupil block is the direct cause of elevated IOP in angle-closure glaucoma. Pupil block refers to the close contact between the pupil and lens, which blocks the AH flowing from the posterior chamber into the anterior chamber through the pupil. Thus, the AH cannot flow out and accumulates in the posterior chamber, leading to elevated IOP.

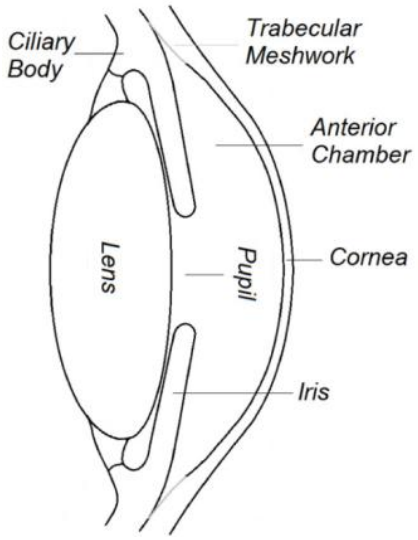

Figure 1. Cyclic process of AH [2].

Laser iridotomy (LI) is the most common surgery for PACG. In LI, the iris is perforated by photothermal effect with the laser incidence angle parallel to the horizontal axis ($\lambda = 0°$) at the mid-peripheral iris, and the AH can enter the anterior chamber through the perforation. By

eliminating the pupil blocking effect, the adhesion of the anterior chamber angle is reduced, and the AH can be expelled smoothly at the trabecular meshwork to alleviate the increase in IOP [3]. Although LI is non-invasive with no risk of intraocular hemorrhage or wound leakage, several complications still occur after surgery, including iris atrophy, corneal endothelial damage, pupillary ectopic deformation, retinal thermal injury, and lens opacity. Corneal endothelial damage may lead to corneal edema and develop into severe bullous keratopathy [4,5]. The occurrence of these complications depends on the anterior chamber depth and IOP at onset and the degree of corneal haziness, but the most critical factors may be the laser parameters in surgery, especially the angle and position in laser drilling [6]. Therefore, studying the influence of laser parameters in surgeries on the AH flow can optimize the operation plan, reduce the occurrence of complications, and provide precise treatment for patients.

The pathogenesis of glaucoma remains unclear. IOP is the only known risk factor for the development of glaucomatous optic neuropathy. Studying the intraocular AH flow plays an important role in controlling the pathogenesis of high IOP glaucoma. However, in clinical settings, the physiological mechanism and pathological changes of the eye cannot be explored through an anatomical analysis of the animal's eyeballs or the intraocular tissues removed from the lesions. The mechanical properties of the wall around the flow field and its velocity, pressure and temperature cannot be measured directly. Consequently, the abovementioned reasons necessitate the numerical simulation of AH flow in the eyeball.

The micro-flow state of intraocular fluid, thermodynamic characteristics, and the regulation mechanism of AH produced by ciliary trabecular meshwork and other organs can be dynamically analyzed and observed. For a long time, the numerical study on AH flow has focused on three aspects: 1) Flow mechanism of AH: the AH flow in the anterior chamber due to saccadic movement was investigated by Abouali et al. [7], in which 3D unsteady flow and energy equation were solved numerically and the saccadic motion was modeled by the dynamic mesh technique. Ooi [8] proposed various hypotheses to describe the cause of AH flow, i.e. the thermally induced flow, AH production and drainage, the mixing and stirring during rapid eye movement sleep, and phacodonesis. Yamamoto and Yasuaki [9] calculated the shear stress exerted on the corneal endothelial cells in anterior chambers with different depths by using a computational fluid dynamics program. They found that the shear stress exerted on CECs after LI may reach a magnitude high enough to cause cell damage and loss in eyes. 2) Resistance of AH outflow: Avtar and Srivastava [10] developed a mathematical model, which treats Schlemm's canal as a porous compliant channel held open by the trabecular meshwork. The IOP and filtration constant have no effect on the pressure distribution in the circular canal, and the volume flux and fluid pressure in the elliptical canal are greater than those in the circular canal. Crowder and Ervin [11] presented a pressure computation for different AH flow rates and viscosities. Numerical results indicated that the difference between the average pressures in the AC and trabecular meshwork increases as the AH viscosity, trabecular meshwork permeability, or AH flow rate increases. 3) Fluid–tissue interaction between the AH and iris: Huang [12] investigated the response of iris contour and curvature to the mechanical interaction between the iris and intraocular structure due to accommodative microfluctuations. Results showed that waveforms of the aqueous–iris mechanical response significantly differ from waveforms of the lens movement for microfluctuations with amplitudes greater than approximately 0.2 D. Wang [13] studied the effects of IOP, localization, and temperature on the AH flow and iris deformation. With the increase in iris elasticity modulus, the equivalent strain and total iris deformation decreases. The maximum

equivalent strain of the iris in the high IOP model is higher than that in the normal IOP model.

To sum up, many efforts have been devoted to analyze AH flow. However, few studies have been conducted on the pathogenesis of high IOP glaucoma and the treatment process of LI. The changes in anterior and posterior chamber pressure *(p*), AH flow velocity (*v*), and consequent AH flow in the entire process of angle-closure glaucoma and LI are not discussed in detail. The angle and position in laser drilling must investigated for individualized and precise treatment to optimize the LI surgical protocols.

Available geometry and mathematical models should be improved to study the entire process further from onset to end of treatment: 1) The anterior chamber of patients with angle-closure glaucoma is often shallow ($H_2 \approx 2.0$ mm), which is not conducive to AH discharge. However, the geometric models established in the literature are normal eyeballs (the anterior chamber depth is H_1 = 2.8–3.0 mm). 2) The existing LI models assume that the natural convection intensity in the anterior chamber is two orders of magnitude larger than the aqueous flow velocity through the pupil. Thus, neither the AH flow in the posterior chamber nor the AH circulation by inflow and outflow pathways is considered. However, during pupil blockade, the gap between the lens and iris (*w*) gradually narrows, which will sharply accelerate the pupil flow speed. Therefore, the influence of the velocity drive of aqueous inlet on the flow field should be considered.

To solve the abovementioned problems, an AH flow domain (anterior and posterior chambers of the eyeball) was modelled using three structures of the eyeball in accordance with the physiological theory of LI treatment, *i.e.*, normal eyeball, eyeball with shallow anterior chamber depth and narrow angle, and eyeball after LI treatment. Finite volume method was used to simulate AH flow under PACG conditions. This work will be helpful in exploring the pathological cause of PACG, preventing the complications of LI, and providing new ideas for clinical guidance.

2. Geometry and mathematical modelling

2.1. Simplified eyeball model

In this work, the anterior part of the eyeball, *i.e.*, the area from the intraocular lens to the cornea, was considered to investigate the AH flow. The model boundaries are the cornea, lens, vitreous body, iris, ciliary body, and trabecular meshwork. Three types of 2D slice eyeball models with different physiological states were established on the basis of the description of glaucoma incidence and laser surgery, namely, eyeball with normal physiological function, eyeball with shallow and narrow chamber angles (the structural premise of glaucoma), and eyeball model after LI (the AH flows into the anterior chamber from the laser hole, and the pupil block is relieved), as shown in Figure 2.

As previously mentioned, the AH secreted by the ciliary body enters the posterior chamber, passes through the pupil between the lens and iris, enters the anterior chamber, and finally leaves the anterior chamber through the trabecular meshwork (Figures 2a and 2b). Figure 2a shows the eyeball model with normal physiological function (anterior chamber depth H_1 = 2.8 mm), whereas Figure 2b presents that with an anterior chamber depth H_2 of 2 mm (the structural premise of glaucoma). When glaucoma develops, the iris–lens channel is closed (w = 0), which blocks the AH flow from the posterior chamber into the anterior chamber through the pupil. The AH that is continuously secreted from the ciliary body will accumulate in the posterior chamber, leading to an elevated posterior chamber pressure and bulged forward iris. However, the AH flow in the affected glaucoma eyeball

cannot be simulated using a computational software because the posterior chamber only has an entrance but no exit. In LI, the iris is perforated by photothermal effect, and the AH can enter the anterior chamber through the perforation, which alleviates the increase in IOP (Figure 2c). In this work, the natural convection caused by the temperature difference between the cornea and internal tissue of the eyeball is considered. The direction of gravity is negative along the Y axis, and g is 9.81 m/s^2.

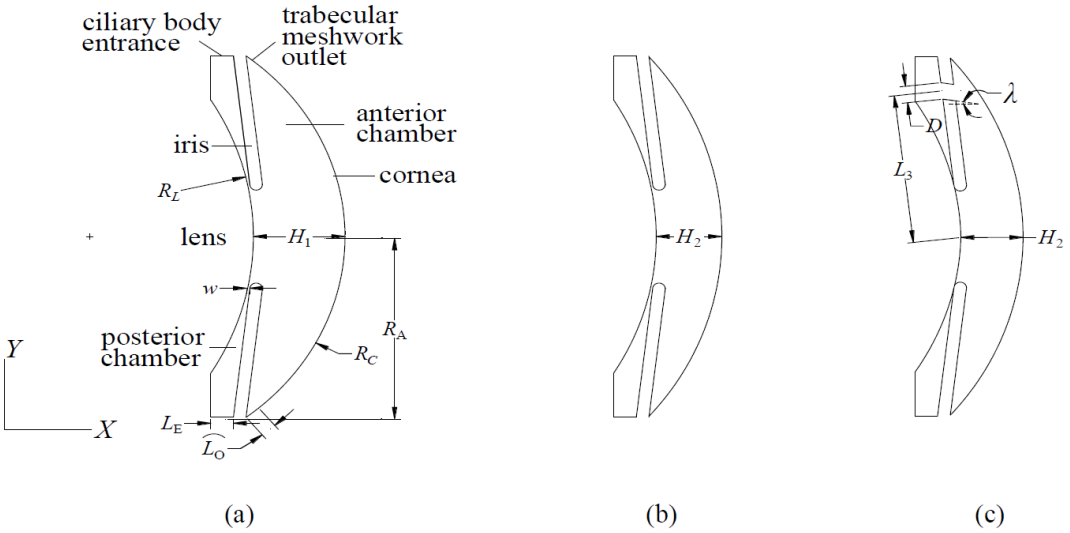

Figure 2. AH cyclic process and geometry model. (a) normal eyeball, (b) eyeball with shallow anterior chamber, and (c) eyeball after LI treatment.

Table 1. Geometric parameters of the tissues [9–13].

Geometric property	Value
Anterior chamber depth of normal eye H_1/mm	2.8
Anterior chamber depth of shallow anterior chamber eye H_2/mm	2.0
Curvature radius of the natural lens R_L/mm	9.0
Minimum curvature radius of the posterior cornea R_C/mm	7.8
Radius of the anterior chamber R_A/mm	6.2
Entrance width of the ciliary body L_E/mm	0.7
Outlet width of the trabecular mesh L_O/mm	0.5
Height of the iris–lens channel w/μm	10, 5, 2, 1, 0.5
Length between the laser hole and pupil axis L_3/mm	5
Diameter of the laser hole D/mm	0.56
Angle between the laser incident direction and pupil axis λ/ °	15 °, 30 °, 45 °, 60 °

Generally, the iris is a flat disk structure, and the posterior surface of the cornea and the anterior capsule of the lens are defined as dome structures. The curvature radii of cornea R_C and lens R_L are 7.8 and 9 mm, respectively. The radius of the entire model R_A is 6.2 mm, the width of the ciliary body entrance L_E is 0.7 mm, and the width of the trabecular meshwork outlet L_O is 0.5 mm. The center distance between the lens and cornea (anterior depth) in the normal eyeball (Figure 2a) H_1 is 2.8 mm, which can represent the size of the normal eyeball. Figures 2(b) and 2(c) uses the

physiological structure of the shallow anterior chamber (H_2 = 2.0 mm) to explore the pathogenesis of angle-closure glaucoma and the principle of surgical treatment further. In Figure 2(c), the cylindrical hole in the iris was utilized to simulate the perforation after laser surgery, with diameter D = 0.56 mm, and was created at the 12 o'clock position of the peripheral iris and the length between the laser hole and pupil axis L_3 = 5 mm [14]. Table 1 summarizes the geometric parameters of the tissues.

2.2. Control equation

The human body is assumed to be standing, so the effect of gravity is considered. AH is regarded as an incompressible Newtonian viscous fluid, and the continuity and momentum equations are as follows:

$$\frac{\partial \rho}{\partial t} + \nabla \bullet (\rho \vec{v}) = 0, \tag{1}$$

$$\frac{\partial \vec{v}}{\partial t} + (\vec{v} \bullet \nabla)\vec{v} + \frac{1}{\rho}\nabla p - \vec{g} - \mu \nabla^2 \vec{v} = 0, \tag{2}$$

Where ρ is the fluid density, t represents the time, v denotes the velocity vector, p indicates the static pressure, g refers to the gravitational acceleration, and μ signifies the fluid kinematic viscosity.

A temperature difference exists between the cornea and human nucleus due to the thermal convection between the cornea and external environment. Therefore, buoyancy-driven natural convection in the anterior chamber is considered by coupling following energy equation:

$$\frac{\partial T}{\partial t} + (\vec{v} \bullet \nabla)T - \frac{k}{\rho c_{\mathrm{p}}}\nabla^2 T - S_T = 0, \tag{3}$$

where T is the temperature; K and c_p stand for the thermal conductivity and specific heat capacity of the fluid, respectively; and S_T denotes the viscous dissipation term. In this study, the heat generation caused by mechanical energy dissipation is neglected.

The main driving force in the anterior chamber is the natural convection caused by temperature difference, and Boussinesq approximation can be used to manage the buoyancy term caused by the thermal natural convection in the enclosed space. In this approximation, 1) the viscous dissipation is neglected, 2) the physical properties are constant except for density, and 3) only the terms related to mass force in the momentum equation are considered for density variation. For the AH fluid, the density is assumed to have a small linear dependence on temperature but independent of pressure:

$$\rho = \rho_{\mathrm{C}}[1 - \alpha(T - T_{\mathrm{C}})], \tag{4}$$

where α is the coefficient of volume expansion. With the Boussinesq approximation, the governing equation can be simplified into

$$\nabla \bullet \vec{v} = 0, \tag{5}$$

$$\rho\vec{v}\bullet\nabla\vec{v}+\nabla p-\rho\vec{g}\alpha(T-T_{\mathrm{C}})-\rho\mu\nabla^2\vec{v}=0\,, \tag{6}$$

$$\rho c_{\mathrm{p}}\vec{v}\bullet\nabla T-k\nabla^2 T=0\,. \tag{7}$$

For the energy equation, the physically realistic and mathematically consistent boundary conditions for the steady problem are prescribed as follows: The outer surface of the cornea has thermal convection with the external environment.

$$-k\frac{\partial T}{\partial n}=h_0(T-T_0)\,, \tag{8}$$

where h_0 is the thermal convection coefficient of the cornea and surrounding environment and T_0 denotes the ambient temperature. The eyeball is assumed to be embedded in a network filled with blood vessels, and its temperature is the same as the core temperature (blood temperature) of the human body due to the circulation of blood inside the capillaries. Therefore, the first type of boundary condition is implemented on the lens and iris with a temperature of 37 ℃.

For the momentum equation, the AH inlet and exit trabecular meshes are considered rigidly permeable boundaries, and the AH tangential velocity at these boundaries is set to zero (no slip). The AH rate is unaffected by the IOP, thereby ensuring the supply of AH inlet flow.

For the normal eyeball (Figure 2a), the aqueous flow rate Q of the normal aqueous circulation is 2.4 μl/min. A velocity boundary condition was adopted to ensure that the flow rate is constant. The velocities are calculated in accordance with the inlet and outlet area ($v = Q/A$). The inlet velocity of the ciliary body is v = 1.990 μm/s, and the outlet velocity of the trabecular meshwork is v = 2.910 μm/s. For the shallow anterior chamber eyeball (Figure 2b), the AH circulation is the same as that of the normal eyeball; thus, their boundary conditions are the same. For the eyeball after LI treatment (Figure 2c), the entrance is the laser hole on the iris, and the exit is the trabecular mesh. By using the particle tracking velocimetry technique, Yamamoto [14] obtained $v_{\max}$ of forward aqueous streaming through the LI window in the eyes (9.39 mm/s). Hence, the inlet condition of the physiological model is v = 9.39 mm/s along the normal direction. The outflow condition is adopted for the trabecular mesh outlet.

Table 2 summarizes the physical properties used in the present model.

Table 2. Physical properties [8,9,11,13].

Physical property	Value
Specific heat capacity C/J(kg·K)$^{-1}$	4178
Density ρ/kg·m^{-3}	1000
Thermal conductivity k/W·(m·K)$^{-1}$	0.58
Dynamic viscosity μ/Pa·s	7.5×10^{-4}
Volume expansion coefficient α/K^{-1}	3.1×10^{-4}
Corneal convection coefficient h_0/W·(m^2·K)$^{-1}$	10

As the Rayleigh number (Ra) is < 10^6, the AH flow is regarded as laminar, which can be solved via the finite volume method in ANSYS Fluent. The momentum and energy equations are discretized

using a second-order upwind scheme, and the SIMPLE algorithm is adopted to decouple the pressure and velocity. A structured grid was applied for the spatial discretization of 2D geometric models. Minimum w = 0.5 μm of the iris–lens channel height H_3 is divided into five grid layers to ensure the computation accuracy, and the total cell number is 20,000–30,000. A grid independence test is performed for all simulations, and the results are reliable.

3. Results and discussion

In this part, the numerical model was initially verified, and then the glaucoma pathogenesis and changes in flow field parameters before and after LI were investigated. This study mainly analyzed the influence of anterior chamber depth on glaucoma pathogenesis, pupil block effect, and AH flow improvement after laser surgery.

3.1. Model verification

The validation of the numerical model is presented in this section. No experimental data are available for AC flow, and the exact solution cannot be derived due to the complexity of the boundary. Therefore, the numerical model was validated in comparison with the theoretical results of Heys [15] (Figure 3).

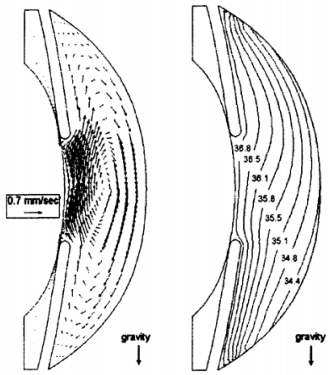

Figure 3. Flow and temperature field by Heys [15].

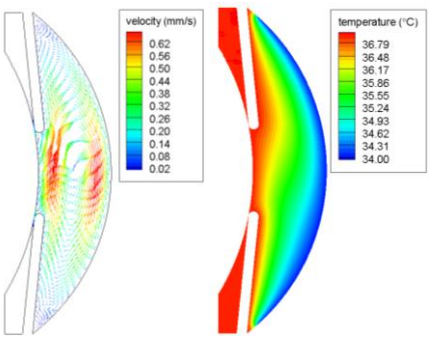

Figure 4. Flow and temperature field in the present simulation.

In this section, the pressure, velocity, and temperature field of the normal eye model are calculated. The corneal temperature is 34 ℃ and w is 5 μm. v_{inlet} and v_{outlet} are 1.990 and 2.910 μm/s, respectively. The flow and temperature fields shown in Figure 4 are compared with the theoretical prediction in Figure 3. The entire velocity vector is consistent, and the peak velocity (0.684 mm/s) is similar to that of Heys (0.7 mm/s). In the temperature field, the isotherms are consistent with that of Heys' study. The isotherms close to the wall are parallel to the wall, which is consistent with the premise that the wall has a constant temperature. Gravity causes asymmetric isotherms, which is consistent with the situation of this study, thereby confirming the model validation.

Two driving forces are available for AH flow: forced convection caused by inlet velocity and natural convection caused by the temperature difference between the cornea and internal tissue of the eyeball. Under a forced convection driven by the inlet velocity, sudden contraction of the cross-sectional area causes a sharp increase in velocity at the gap between the iris and lens with a maximum velocity of 0.3 mm/s. The temperature difference between the cornea and internal tissue produces vertical buoyancy, thereby yielding natural convection in the anterior chamber. The increase in velocity is due to the coupling of forced convection with natural convection. The temperature field slightly tilts due to the forced convection. The larger the flow velocity in the anterior chamber, the greater the inclination of the temperature field. Therefore, the consideration of theforced convection caused by the inlet velocity can obtain a further accurate flow field.

3.2. Influence of anterior chamber depth

Existing studies on AH flow have focused on normal eyeballs. However, glaucoma is characterized by a shallow anterior chamber depth. Therefore, the flow field in non-onset glaucoma with shallow depth H_2 = 2.0 mm was compared with that of the normal eyeball (anterior chamber depth H_1 = 2.8 mm) to explore the influence of physiological structure on the AH flow with similar boundary conditions in Section 3.1.

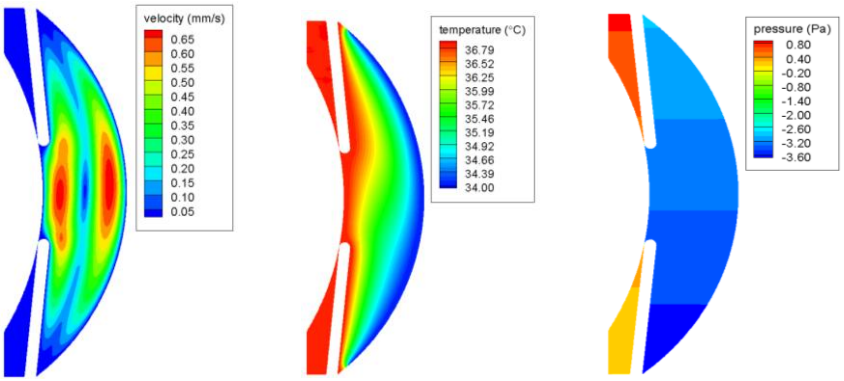

(a) (b) (c)

Figure 5. AH flow with the normal eyeball. (a) the flow field, (b) the temperature field, and (c) the pressure field.

Figure 6 shows the velocity, temperature, and pressure field in the eyeball with shallow anterior chamber, which is similar to those of the normal eyeball (Figure 5). The same tendency is observed,

but the parameter changes greatly. The peak velocity of the normal eye is 0.686 mm/s, whereas that of the shallow anterior chamber is only 0.32 mm/s (decreases by half), with unchanged velocity at the narrowest position between the lens and iris. However, less mixing and stirring for driving the flow in the area are observed due to the low velocity in the shallow anterior chamber. When the temperature difference is constant, the vortex generated by natural convection is affected by the wall. If the anterior chamber becomes small, then the space is insufficient for full development, thereby decreasing the speed. A small natural convection intensity will also result in parallel isotherms to the wall (Figure 6). Meanwhile, the pressure difference between the shallow anterior chamber and posterior chamber increases by 20% (from 3.8 Pa to 5 Pa). As such, the shallow anterior chamber depth is crucial for the accurate investigation of glaucoma.

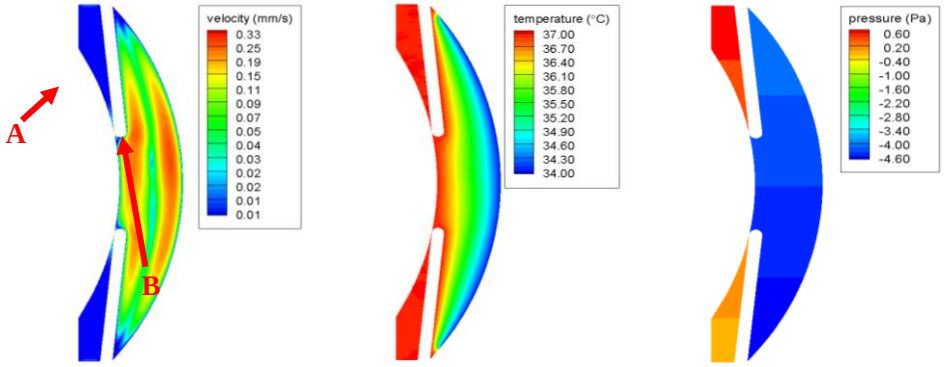

(a) (b) (c)

Figure 6. AH flow with the shallow anterior chamber. (a) the flow field, (b) the temperature field, and (c) the pressure field.

3.3. Pupil block effect

Pupil block is the direct cause of elevated IOP in angle-closure glaucoma. In this section, AH flow characteristics with different w values (10, 5, 2, 1, and 0.5 μm) are analyzed to mimic the real eyeball structure of glaucoma patients. Through a simulation during pupil block, we can further understand the pupil block effect in the pathogenesis of glaucoma to improve the operation plan and avoid complications.

The pressure difference between the anterior and posterior chambers ΔP, velocity v_A at the narrowest point between the iris and lens (point A in Figure 6), and maximum velocity v_B in the anterior chamber caused by natural convection (point B in Figure 6) are compared in Figures 7 and 8. v_A increases sharply with the decrease in w, whereas v_B increases slightly. As the flow rate of AH is constant, v increases sharply when cross-section area A decreases rapidly. v_B represents the coupling of forced convection with natural convection; its slight increase is caused by the increase in forced convection velocity (the intensity of natural convection remains unchanged).

ΔP increased sharply with the decrease in w. When the minimum w is more than 5 μm, ΔP has no physiological significance to the eyeball tissue. When w is 0.5 μm, ΔP increases significantly, that is, approximately 37 times of that at w = 10 μm. When the degree of pupil block increases, the gap between the lens and iris can be predicted to decrease continuously. The AH cannot flow through the pupil, and an extremely high ΔP will push the iris forward, close the anterior chamber angle, and

increase the IOP. A high IOP in the anterior part of the eye transmits to surrounding tissues, thereby causing damage to the retina of the fundus and changing the visual field, eventually leading to blindness.

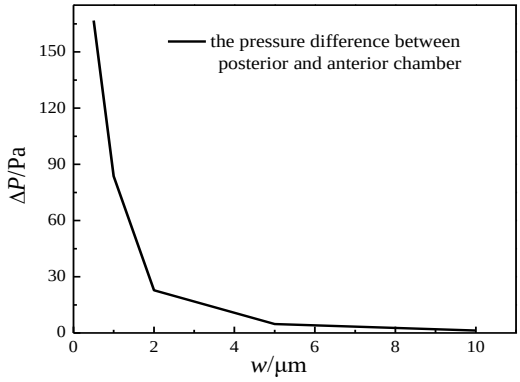

Figure 7. Pressure difference.

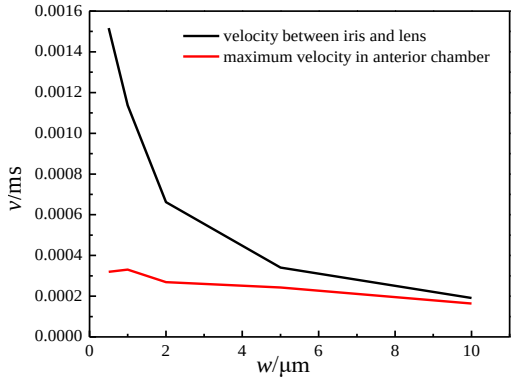

Figure 8. Maximum velocity.

3.4. Improvement of AH flow after laser surgery

This section simulates AH flow characteristics after laser surgery to understand the flow improvement and attempt to prevent the occurrence of complications by changing the operation parameters. The laser hole is at the 12 o'clock position of the peripheral iris and 5 mm from the pupil axis. When the LI window diameter (D) is 0.56 mm, the initial velocity through the LI window is set to 9.39 mm/s and then decays in the form of a cosine function [14]. When the newly established aqueous water enters the steady state (the inlet and outlet flows are equal), the inlet velocity of the laser hole is 1.17 mm/s.

Figure 9 shows the AH flow field immediately after laser perforation. After laser perforation, the AH fluid accumulated in the posterior enters the anterior chamber through the laser hole, effectively alleviating the high IOP caused by pupil block, and the IOP decreases from an order of kPa to a normal level (Pa). However, the velocity near the laser hole is increased, and the produced

jet velocity is higher than the maximum velocity in the anterior chamber when the iris is not perforated (increased by 40 times). Thus, the shear stress will increase when the AH jet affects the cornea, thereby causing its mechanical damage. As the entrance velocity is two orders of magnitude larger than the natural convection velocity, natural convection in the anterior chamber can be neglected. At this time, heat is transferred from the posterior part to the anterior part of the eye through thermal convection, which increases the AH temperature near the laser hole.

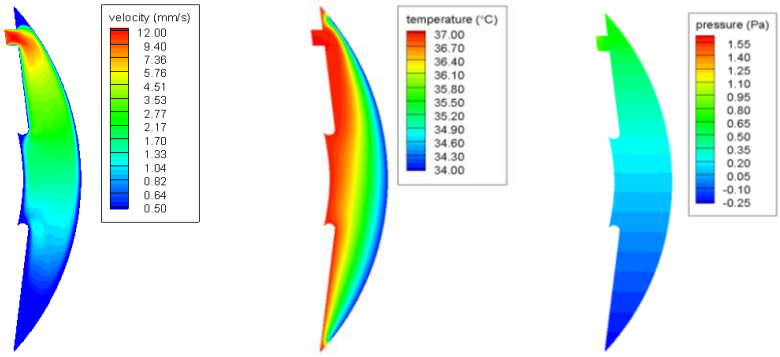

(a) (b) (c)

Figure 9. AH flow characteristics after LI. (a) the flow field, (b) the temperature field, and (c) the pressure field.

Figure 10 shows the distribution of the wall shear stress under different conditions: normal aqueous circulation (ciliary body–posterior chamber–pupil–anterior chamber–trabecular mesh) with inlet velocity v_{in} = 1.990 μm/s in Figure 10a, with initial inlet velocity of 9.39 mm/s (maximum velocity after laser drilling) in Figure 10b, and after stabilization of the new aqueous circulation (ciliary body–posterior chamber–laser orifice–anterior chamber–trabecular mesh) with v_{in} = 1.17 mm/s in Figure 10c. The corneal shear stress is 1.02 mPa, and the iris shear stress is 200 mPa in normal aqueous circulation (Figure 10a). At the instant of laser perforation, the corneal shear stress is 43.06 mPa, which is 40 times that of the normal aqueous circulation, and the iris shear stress reaches 450 mPa. After the postoperative flow field is stabilized, the corneal shear stress recovers to 5.56 mPa, and the iris shear stress is 61 mPa. Although the shear stress is reduced compared with that in Figure 10b, it is still 5.5 times the corneal shear stress in the normal aqueous circulation, thereby causing damage to the cornea. Youm et al. [16] performed LI on the right eyes of pigmented rabbits. They found that LI induces corneal endothelial cell apoptosis and results in decreased endothelial cell density. Priscilla [17] indicated that the longest reported interval between the LI and corneal decompensation is 8 years. These studies showed that the LI's mechanical damage to the cornea does not only exist during surgery, but the effect of AH will damage the cornea for a long time.

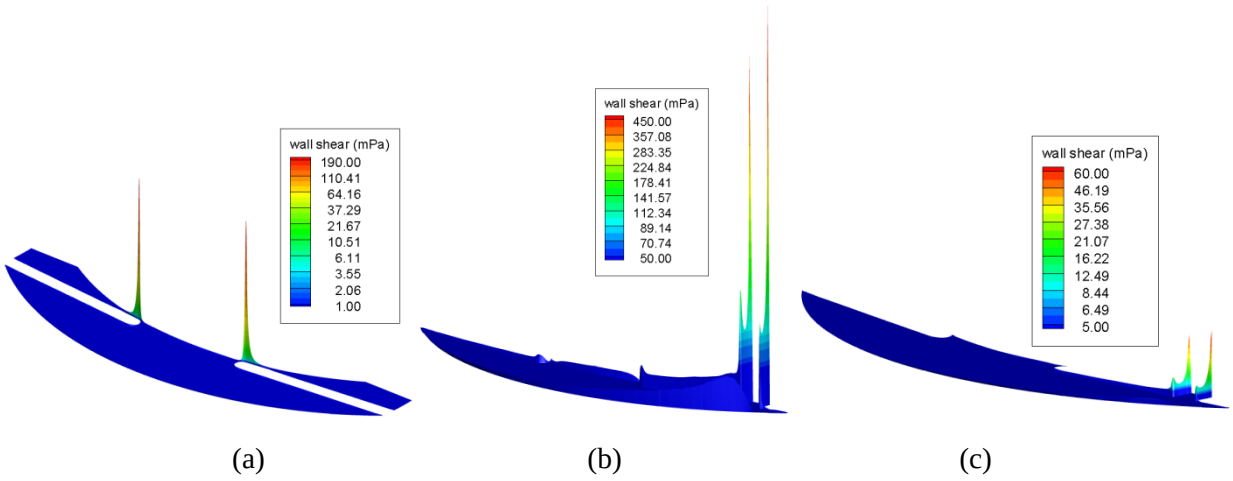

Figure 10. AH flow characteristics after LI. (a) normal aqueous circulation, (b) initial entrance velocity after laser drilling, (c) new aqueous circulation after LI.

To avoid corneal mechanical damage and complications, such as corneal edema, after LI, the influence of laser parameters in surgeries on the AH flow field was studied to reduce the effect of AH flow on the cornea and depress the corneal shear stress. The laser parameters (energy density, spot size, and pulse duration) can be adjusted in LI to achieve different iris drilling effects, which are embodied in the size (D), angle (λ), and position (L_3) of the laser hole, as shown in Figure 2c. The location of the laser hole is generally set at the mid-peripheral iris, which can avoid laser irradiation of the iris crystal contact area to prevent crystal damage. However, if the location is in excessive periphery, obstacles to the arcus senilis may appear, thereby increasing the risk of burning the cornea. The location of the iris crypt should be selected when possible, because the iris is thin and easy to penetrate. The size of laser perforation D is related to the laser energy. Enlarging the aperture will reduce the AH jet effect after opening. If the cauterization time is long, then the laser energy may cause complications, such as iris charring, corneal thermal damage, and crystal turbidity, and diplopsia and dazzle may occur. Therefore, the position and size of laser iris drilling cannot be changed at will.

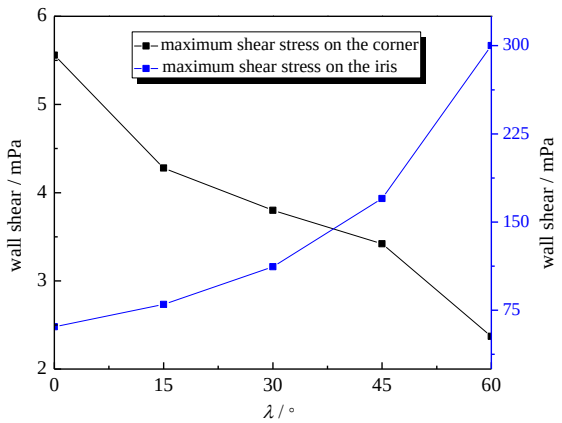

Figure 11. Maximum wall shear stress under different drilling angles.

In previous operations, laser beams were incident parallel to the horizontal axis ($\lambda = 0°$). This study innovatively suggested that laser beams should incident to the eyeball at a certain angle in LI, so that the orientation of the laser hole on the iris has a certain angle with the horizontal direction (x axis, as shown in Figure 2c). This approach can avoid the lens damage caused by the laser energy directly acting on the lens after the beam penetrated the iris and impede crystal turbidity. Moreover, it can be prevented from directly affecting the AH on the nearby cornea because of the oblique incidence into the anterior chamber.

On this basis, wall shear stress at different drilling angles was explored. As the overall distribution trend of wall shear stress is the same under different drilling angles (Figures 10b and 10c), the location of the maximum corneal shear stress is perpendicular to the aqueous flow jet. Hence, the shear stress distribution diagrams under different working conditions are not presented here. Figure 11 shows the maximum shear stress on the corner and iris under different drilling angles ($\lambda = 15°, 30°, 45°, 60°$). A large angle may break down the iris with a large scope of iris thermal injury. By contrast, a small laser drilling angle will lead to lens damage and corneal mechanical injury. The maximum shear stress of the cornea decreases, and the shear stress of the iris increases as the drilling angle increases.

Three criteria are available to determine the optimal drilling angle: 1) reducing the shear stress of aqueous jet on the cornea, 2) reducing the shear stress on the iris, and 3) the allowable angle range of surgical equipment. For criterion 1, the larger the drilling angle, the smaller the corneal shear stress, and the smaller the mechanical damage. For criterion 2, the influence of the optimal angle on the shear stress can be ignored because even the maximum shear stress of the iris is too small compared with the mechanical damage threshold of the iris (the elastic modulus K of the iris is 9 kPa [2]). For criterion 3, the deflection angle λ of the iris aperture in laser shooting is 0°–50° [18]. The reason is that LI is often performed by covering an anti-reflective coated contact lens. The influence of eye movement on accurate laser shooting can be reduced by controlling the contact lens, which is helpful for eyelid separation, laser beam focusing, and tissue enlargement in the treatment. On the basis of the previous analysis, the optimum laser aperture angle λ is 45°. That is, the deflection angle of the laser beam allowed by the operating equipment can also effectively reduce the corneal shear stress and mechanical damage. Meanwhile, shooting iris at a certain angle can avoid lens damage and complications, such as lens opacity.

4. Conclusion

In this study, the AH flow was modelled through three structures of the eyeball in accordance with the physiology of PACG. The finite volume method was used to simulate the AH flow. Results showed that:

(1) The geometric model of the physiological structure of the shallow anterior chamber depth is crucial for the theoretical study of glaucoma. When the anterior chamber depth decreases from 2.8 mm to 2.0 mm, the maximum velocity of natural convection doubles, and the pressure difference of the shallow anterior chamber increases by 20%.

(2) Pupil block sharply increases the IOP. When $w = 0.5$ μm, ΔP is approximately 37 times that at $w = 10$ μm, and a high ΔP will cause damage to the intraocular tissues.

(3) LI can effectively reduce the IOP caused by pupil block. However, the AH velocity after operation is 40 times the normal speed, and the increase in corneal shear stress can result in

corneal damage.

(4) Laser shooting iris at a certain angle can not only avoid the lens damage caused by the laser energy directly acting on the lens after the laser beam penetrated the iris but also prevent the direct effect of the AH flow jet on the cornea near the anterior chamber and reduce the corneal mechanical damage. On the basis of the allowable angle range of the surgical equipment and the effect of different incident angles on the cornea and iris, the optimum angle of laser drilling is 45 °.

Although laser shooting iris at a certain angle is allowed by the instruments in clinical surgery, there are still no relevant experiments and literature reports. In future, we will carry out experimental verification on rabbit eyes to obtain the flow field characteristics and wall shear stress, which will make this conclusion more rigorous and practical.

Acknowledgments

This work was supported by the National Natural Science Foundation of China (51727811).

Conflict of interest

The authors declare no conflict of interest in this paper.

References

1. S. Zhang, C. Wu, L. Liu, et al., Optical coherence tomography angiography of the peripapillary retina in primary angle-closure glaucoma, *Am. J. Ophthalmol.*, **182** (2017), 194.
2. J. Sara, A. Rouzbeh and V. H. Barocas, Contribution of different anatomical and physiologic factors to iris contour and anterior chamber angle changes during pupil dilation: theoretical analysis, *Invest. Ophth. Vis. Sci.*, **54** (2013), 2977–2984.
3. F. Zhang and H. Chen, Numerical investigation of laser iridotomy influence on shear stress exerted on corneal endothelial cells, *J. Med. Biomech.*, (2016).
4. L. W. Schwartz and G. L. Spaeth, Argon laser iridotomy in primary angle-closure or pupillary block glaucoma, *Laser. Surg. Med.*, **1** (2010), 153–164.
5. N. Satoru and M. Akira, Three-year outcome of Descemet stripping automated endothelial keratoplasty for bullous keratopathy after argon laser iridotomy, *Cornea*, **33** (2014), 780–784.
6. O. V. Danilenko and A. V. Bol'Shunov, Laser iridectomy and anatomical and functional parameters in primary angle-closure glaucoma, *Vestnik Oftalmologii*, **130** (2014), 54.
7. O. Abouali, A. Modareszadeh, A. Ghaffarieh, et al., Investigation of saccadic eye movement effects on the fluid dynamic in the anterior chamber, *J. Biomech. Eng.*, **134** (2012), 021002.
8. E. H. Ooi and E. Y. K. Ng, Effects of natural convection within the anterior chamber on the ocular heat transfer, *Int. J. Numer. Meth. Bio. Eng.*, **27** (2015), 408–423.
9. Y. Yasuaki, U. Toshihiko, J. Takeshi, et al., Effect of anterior chamber depth on shear stress exerted on corneal endothelial cells by altered aqueous flow after laser iridotomy, *Invest. Ophth. Vis. Sci.*, **51** (2010), 1956.
10. R. Avtar and R. Srivastava, Aqueous outflow in Schlemm's canal, *Appl. Math. Comput.*, **174** (2006), 316–328.

11. T. R. Crowder and V. J. Ervin, Numerical simulations of fluid pressure in the human eye, *Appl. Math. Comput.*, **219** (2013), 11119–11133.
12. E. C. Huang and V. H. Barocas, Accommodative microfluctuations and iris contour, *J. Vision*, **6** (2006), 653.
13. W. Wang, X. Qian, H. Song, et al., Fluid and structure coupling analysis of the interaction between aqueous humor and iris, *Biomed. Eng. Online*, **15** (2016), 133.
14. Y. Yasuaki, U. Toshihiko, S. Katsumi, et al., Demonstration of aqueous streaming through a laser iridotomy window against the corneal endothelium, *Arch. Ophthalmol.*, **124** (2006), 387.
15. J. J. Heys, V. H. Barocas and M. J. Taravella, Modeling passive mechanical interaction between aqueous humor and iris, *J. Biomech. Eng.*, **123** (2001), 540.
16. H. Y. Jie, J. H. Heo, H. M. Kim, et al., Effects of Argon Laser Iridotomy on the Corneal Endothelium of Pigmented Rabbit Eyes, *Korean J. Ophthalmol.*, **28** (2014), 76–82.
17. P. X. Wang, V. T. C. Koh and L. S. Chee, Laser iridotomy and the corneal endothelium: a systemic review, *Acta Ophthalmol.*, **92** (2015), 604–616.
18. R. Y. Lee, K. Toshimitsu, N. Q. Cui, et al., Association between baseline angle width and induced angle opening following prophylactic laser peripheral iridotomy, *Invest. Ophth. Vis. Sci.*, **54** (2013), 3763–3770.

AIMS Press